Paper 247

Proceedings of the Eleventh International Conference
on Computational Structures Technology,
B.H.V. Topping, (Editor),
Civil-Comp Press, Stirlingshire, Scotland

Thermo-Mechanical Analysis of Isotropic and Orthotropic Beams using a Unified Formulation

D. Crisafulli[1,2], G. Giunta[2], E. Carrera[1] and S. Belouettar[2]
[1] Department of Mechanical and Aerospace Engineering
Politecnico di Torino, Italy
[2] Department of Advanced Materials and Structures, Centre de Recherche
Public Henri Tudor, Luxembourg-Kirchberg, Luxembourg

Abstract

In this paper the deformations of simply supported isotropic and orthotropic beams subjected to thermal loadings are analysed. The governing equations are derived from the principle of virtual displacements accounting for the temperature as an external laod only. The required temperature field is not assumed a priori, but is determined solving Fourier's heat conduction equation. Numerical results for temperature, displacemnts and stress distributions are provided for different beam slenderness ratios. Comparison with three-dimensional finit element models is given.

Keywords: thermal load, beam structure, refined models, closed form solution, unified formulation, principle of virtual displacements.

1 Introduction

Many tipical aeronautical and space structures concern isotropic and composite beam-like structures that must operate in complex environment. In particular the severe temperature loads involved in many engineering applications require the development of refined models for their analysis. Several application of the theory of thermoelasticity can be found in the book of Hetnarski and Eslami [1]. In particular, the thermal stress analysis of beams based on Euler-Bernoulli assumptions was presented. The thermo-elastic stress analysis of multilayered beams was carried out by Carpinteri and Poggi in [2]. Analytical solution were given under the Euler-Bernoulli hypotheses, when rigid interfaces between the layers were taken into account. A finite element semi-discretisation for composite beams was presented by Ghiringhelli [3]. The temperature distribution within the beam cross-section was computed by a two-dimensional finite element procedure. The structural thermo-elastic problem was discussed and comparison with three-dimensional finite element analysis were presented. Beams

with variable thickness and subjected to thermo-mechanical loads were investigated in the work of Xu and Zhou [4]. The non-linear temperature profile along the beam's thickness was computed solving the heat conduction equation. Results were compared with those obtained from the commercial finite element software ANSYS. A three-noded thermomechanical beam finire element for the analysis of laminated beam was derived by Vidal and Polit [5]. Kapuria et al. [6] preented a higher order zigzag theory for thermal stress analysis of laminated beams under thermal loads. The thermal field is approximated as piecewise linear across the thickness. The governing equations are derived using the principle of virtual work and Fourier series solutions are obtained for simply-supported beams. Tanigawa et al. [7] consider the transient thermal stress analysis of a laminated beam. The heat conduction problem is treated as one-dimensional in the thickness direction. The thermal stress distributions was obtained using the elementary beam theory and Airy's thermal stress function method. Sayman [8] studied the elasto-plastic thermal behavior of steel fiber-reinforced aluminium metal-matrix composite beams. Linear variation of the temperature is taken into account. The thermal response of orthotropic laminated plates was investivated by Carrera [9], through the comparison between theories formulated on the basis of the principle of virtual displacements (PVD) and mixed theories based on the Reissner mixed variational theorem (RMVT). The effect of the through-the-thickness temperature profile on the accuracy of classical and advanced plate theories was studied by Carrera in [10]. A thermal analysis of isotropic and composite beams via refined models is addressed in this paper. Models are derived via a Unified Formulation (UF) that has been previously formulated for plates and shells, (see Carrera [11]) and extended to solid and composite beams (see Carrera et al. [12] and Catapano et al. [13]). In the Unified Formulation the dislacements' assumptions are written in a compact form. The governing equations variationally consistent with the made hypothesis are derived through the Principle of Virtual Displacements, in terms of fundamental nucleo. This is a free parameter of the formulation, since it does not depend upon the order of expansion. As a result, an exhaustive variable kinematic model can be obtained that accounts for transverse shear deformability and cross-section in- and out-of-plane warping. The temperature field is descibed in the same way as the displacements, or rather splitted in a set of cross-section functions and the relative terms depending on the beam axis x coordinate only. Governing differential equations are solved via a Navier, closed form solution. Slender and deep beams, as well as isotropic and orthotropic materials, are investigated. The results obtained through the proposed formulation have been compared with three-dimensional FEM models. When the appropriate expansion order is considered, achieved results are in agreement with the FEM's one.

2 Preliminaries

A beam is a structure whose axial extension (l) is predominant if compared to any other dimension orthogonal to it. The cross-section (Ω) is identified by intersecting the beam with planes that are orthogonal to its axis. A Cartesian reference system is

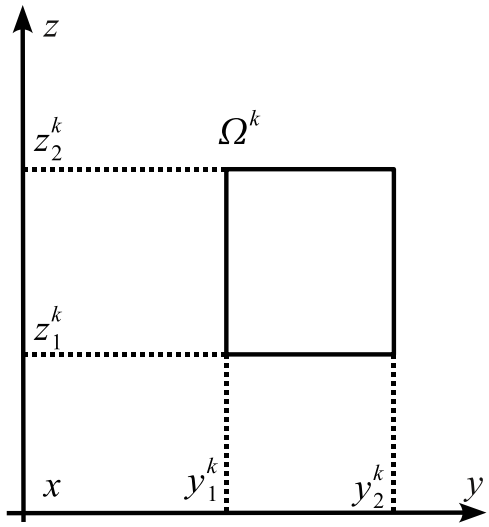

Figure 1: Beam cross-section geometry and reference system.

adopted: y- and z-axis are two orthogonal directions laying on Ω. The x coordinate is coincident to the axis of the beam. It is bounded such that $0 \leq x \leq l$. Cross-section geometry and reference system are reported in Figure 1.

The cross-section is considered to be constant along x. The displacement field is:

$$\mathbf{u}^T(x,y,z) = \left\{ \begin{array}{ccc} u_x(x,y,z) & u_y(x,y,z) & u_z(x,y,z) \end{array} \right\} \tag{1}$$

in which u_x, u_y and u_z are the displacement components along x-, y- and z-axes. Superscript 'T' represents the transposition operator. Stress, $\boldsymbol{\sigma}$, and strain, $\boldsymbol{\varepsilon}$, vectors are grouped into vectors $\boldsymbol{\sigma}_n$, $\boldsymbol{\varepsilon}_n$ that lay on the cross-section:

$$\boldsymbol{\sigma}_n^T = \left\{ \begin{array}{ccc} \sigma_{xx} & \sigma_{xy} & \sigma_{xz} \end{array} \right\} \quad \boldsymbol{\varepsilon}_n^T = \left\{ \begin{array}{ccc} \varepsilon_{xx} & \varepsilon_{xy} & \varepsilon_{xz} \end{array} \right\} \tag{2}$$

and $\boldsymbol{\sigma}_p$, $\boldsymbol{\varepsilon}_p$ laying on planes orthogonal to Ω:

$$\boldsymbol{\sigma}_p^T = \left\{ \begin{array}{ccc} \sigma_{yy} & \sigma_{zz} & \sigma_{yz} \end{array} \right\} \quad \boldsymbol{\varepsilon}_p^T = \left\{ \begin{array}{ccc} \varepsilon_{yy} & \varepsilon_{zz} & \varepsilon_{yz} \end{array} \right\} \tag{3}$$

Under the hypothesis of linear analysis, the following total strain-displacement geometrical relations hold:

$$\begin{array}{c} \boldsymbol{\varepsilon}_n^T = \left\{ \begin{array}{ccc} u_{x,x} & u_{x,y} + u_{y,x} & u_{x,z} + u_{z,x} \end{array} \right\} \\ \boldsymbol{\varepsilon}_p^T = \left\{ \begin{array}{ccc} u_{y,y} & u_{z,z} & u_{y,z} + u_{z,y} \end{array} \right\} \end{array} \tag{4}$$

Subscripts 'x', 'y' and 'z', when preceded by comma, represent derivation versus the corresponding spatial coordinate. A compact vectorial notation can be adopted for Equation (4):

$$\begin{array}{c} \boldsymbol{\varepsilon}_n = \mathbf{D}_{np}\mathbf{u} + \mathbf{D}_{nx}\mathbf{u} \\ \boldsymbol{\varepsilon}_p = \mathbf{D}_p\mathbf{u} \end{array} \tag{5}$$

where $\mathbf{D}_{np}$, $\mathbf{D}_{nx}$, and $\mathbf{D}_p$ are the following differential matrix operators:

$$\mathbf{D}_{np} = \begin{bmatrix} 0 & 0 & 0 \\ \dfrac{\partial}{\partial y} & 0 & 0 \\ \dfrac{\partial}{\partial z} & 0 & 0 \end{bmatrix} \quad \mathbf{D}_{nx} = \mathbf{I}\frac{\partial}{\partial x} \quad \mathbf{D}_p = \begin{bmatrix} 0 & \dfrac{\partial}{\partial y} & 0 \\ 0 & 0 & \dfrac{\partial}{\partial z} \\ 0 & \dfrac{\partial}{\partial z} & \dfrac{\partial}{\partial y} \end{bmatrix} \tag{6}$$

$\mathbf{I}$ is the unit matrix. In the case of thermo-mechanical problems, the constitutive equations are given as:

$$\begin{aligned} \boldsymbol{\sigma}_p &= \boldsymbol{\sigma}_{pd} - \boldsymbol{\sigma}_{pt} = \widetilde{\mathbf{C}}_{pp}\boldsymbol{\varepsilon}_p + \widetilde{\mathbf{C}}_{pn}\boldsymbol{\varepsilon}_n - \widetilde{\lambda}_p(y,z)T \\ \boldsymbol{\sigma}_n &= \boldsymbol{\sigma}_{nd} - \boldsymbol{\sigma}_{nt} = \widetilde{\mathbf{C}}_{np}\boldsymbol{\varepsilon}_p + \widetilde{\mathbf{C}}_{nn}\boldsymbol{\varepsilon}_n - \widetilde{\lambda}_n(y,z)T \end{aligned} \tag{7}$$

where suscript d and t refer to the mechanical and the thermal contributions, respectively. Matrices $\widetilde{\mathbf{C}}_{pp}$, $\widetilde{\mathbf{C}}_{pn}$, $\widetilde{\mathbf{C}}_{np}$ and $\widetilde{\mathbf{C}}_{nn}$ in Eqs. (7) are:

$$\begin{gathered} \widetilde{\mathbf{C}}_{pp} = \begin{bmatrix} \widetilde{C}_{22} & \widetilde{C}_{23} & 0 \\ \widetilde{C}_{23} & \widetilde{C}_{33} & 0 \\ 0 & 0 & \widetilde{C}_{44} \end{bmatrix} \quad \widetilde{\mathbf{C}}_{pn} = \widetilde{\mathbf{C}}_{np}^T = \begin{bmatrix} \widetilde{C}_{12} & 0 & 0 \\ \widetilde{C}_{13} & 0 & 0 \\ 0 & 0 & 0 \end{bmatrix} \\ \widetilde{\mathbf{C}}_{nn} = \begin{bmatrix} \widetilde{C}_{11} & 0 & 0 \\ 0 & \widetilde{C}_{66} & 0 \\ 0 & 0 & \widetilde{C}_{55} \end{bmatrix} \end{gathered} \tag{8}$$

The material stiffness coefficents $\widetilde{\mathbf{C}}_{ij}$ are rotated in order to consider the fiber orientation respect to the x, y plane. The temperature is here seen as:

$$T(x,y,z) = \Theta_n(x)\Theta_\Omega(y,z) \tag{9}$$

where $\Theta_n(x)$ is the temperature variation respect to the beam axis coordinate x and $\Theta_\Omega(y,z)$ is the temperature variation respect to the beam cross-sections coordinates y, z. The coefficients $\widetilde{\lambda}_p(y,z)$ and $\widetilde{\lambda}_n(y,z)$ are:

$$\widetilde{\boldsymbol{\lambda}}_n^T = \left\{ \begin{array}{ccc} \widetilde{\lambda}_{xx} & \widetilde{\lambda}_{xy} & \widetilde{\lambda}_{xz} \end{array} \right\} \quad \widetilde{\boldsymbol{\lambda}}_p^T = \left\{ \begin{array}{ccc} \widetilde{\lambda}_{yy} & \widetilde{\lambda}_{zz} & \widetilde{\lambda}_{yz} \end{array} \right\} \tag{10}$$

and are linked to the coefficients of thermal expansion $\widetilde{\alpha}_p$ and $\widetilde{\alpha}_n$:

$$\widetilde{\boldsymbol{\alpha}}_n^T = \left\{ \begin{array}{ccc} \widetilde{\alpha}_{xx} & \widetilde{\alpha}_{xy} & \widetilde{\alpha}_{xz} \end{array} \right\} \quad \widetilde{\boldsymbol{\alpha}}_p^T = \left\{ \begin{array}{ccc} \widetilde{\alpha}_{yy} & \widetilde{\alpha}_{zz} & \widetilde{\widetilde{\alpha}}_{yz} \end{array} \right\} \tag{11}$$

through the following Equations:

$$\begin{aligned} \widetilde{\boldsymbol{\lambda}}_p &= \widetilde{\mathbf{C}}_{pp}\widetilde{\boldsymbol{\alpha}}_p + \widetilde{\mathbf{C}}_{pn}\widetilde{\boldsymbol{\alpha}}_n \\ \widetilde{\boldsymbol{\lambda}}_n &= \widetilde{\mathbf{C}}_{np}\widetilde{\boldsymbol{\alpha}}_p + \widetilde{\mathbf{C}}_{nn}\widetilde{\boldsymbol{\alpha}}_n \end{aligned} \tag{12}$$

In the present model, the temperature is seen as an external loading, once its variation on the beam has been obtained by solving Fourier's heat conduction equation.

3 Hierarchical beam theories

The variation of the displacement field over the cross-section can be postulated a-priori. Several displacement-based theories can be formulated on the basis of the following generic kinematic field:

$$\mathbf{u}\left(x,y,z\right)=F_{\tau}\left(y,z\right)\mathbf{u}_{\tau}\left(x\right)\ \text{ with }\ \tau=1,\ 2,\ \ldots,\ N_{u} \tag{13}$$

N_u stands for the number of unknowns. It depends on the approximation order N that is a free parameter of the formulation. The compact expression is based on Einstein's notation: subscript τ indicates summation. Thanks to this notation, problem's governing differential equations and boundary conditions can be derived in terms of a single 'fundamental nucleo'. The complexity related to higher than classical approximation terms is tackled and the theoretical formulation is valid for the generic approximation order and approximating functions $F_{\tau}\left(y,z\right)$. In this paper, the functions F_{τ} are assumed to be Mac Laurin's polynomials. This choice is inspired by the classical beam models. The actual governing differential equations and boundary conditions due to a fixed approximation order and polynomials type are obtained straightforwardly via summation of the nucleo corresponding to each term of the expansion. The generic N-order displacement field is:

$$\begin{aligned}
u_x &= u_{x1}+u_{x2}y+u_{x3}z+\cdots+u_{x\frac{(N^2+N+2)}{2}}y^N+\cdots+u_{x\frac{(N+1)(N+2)}{2}}z^N\\
u_y &= u_{y1}+u_{y2}y+u_{y3}z+\cdots+u_{y\frac{(N^2+N+2)}{2}}y^N+\cdots+u_{y\frac{(N+1)(N+2)}{2}}z^N\\
u_z &= u_{z1}+u_{z2}y+u_{z3}z+\cdots+u_{z\frac{(N^2+N+2)}{2}}y^N+\cdots+u_{z\frac{(N+1)(N+2)}{2}}z^N
\end{aligned} \tag{14}$$

Classical models, such as Timoshenko beam theory (TB) and Euler-Bernoulli beam theory (EB) are straightforwardly derived from the first-order approximation model. In TB, no shear correction coefficient is considered, since it depends upon several parameters, such as the geometry of the cross-section (see, for instance, Cowper [14] and Murty [15]). Higher order models yield a more detailed description of the shear mechanics (no shear correction coefficient is required), of the in- and out-of-section deformations, of the coupling of the spatial directions due to Poisson's effect and of the torsional mechanics than classical models do. EB theory neglects them all, since it was formulated to describe the bending mechanics. TB model accounts for constant shear stress and strain components. In the case of classical models and first-order approximation, the material stiffness coefficients should be corrected in order to contrast a phenomenon known in literature as Poisson's locking (see Carrera and Brischetto [16, 17]).

4 Governing equations

The derivation of the governing equations and the boundary conditions is based on the principle of virtual displacements (PVD):

$$\delta L_i=0 \tag{15}$$

δ stands for a virtual variation. L_i represents the strain energy. No external work is considered.

4.1 Virtual variation of the strain energy

According to the grouping of the stress and strain components in Equations (2) and (3), the virtual variation of the strain energy is considered as sum of two contributes:

$$\delta L_i = \int_l \int_\Omega \left[\delta \boldsymbol{\epsilon}_n^T \boldsymbol{\sigma}_n + \delta \boldsymbol{\epsilon}_p^T \boldsymbol{\sigma}_p \right] d\Omega dx \tag{16}$$

For the thermo-mechanical case, it reads:

$$\delta L_i = \int_l \int_\Omega \left[\delta \boldsymbol{\epsilon}_n^T (\boldsymbol{\sigma}_{nd} - \boldsymbol{\sigma}_{nt}) + \delta \boldsymbol{\epsilon}_p^T (\boldsymbol{\sigma}_{pd} - \boldsymbol{\sigma}_{pt}) \right] d\Omega dx \tag{17}$$

By substitution of the geometrical relations (5), the constitutive equations (7), and the unified hierarchical approximation of the displacements ((13), and after integration by parts, Equation (17) becomes:

$$\begin{aligned}
\delta L_i = \int_l \delta \mathbf{u}_\tau^T \int_\Omega \Big[& (\mathbf{D}_{np} F_\tau)^T \widetilde{\mathbf{C}}_{np} (\mathbf{D}_p F_s) + (\mathbf{D}_{np} F_\tau)^T \widetilde{\mathbf{C}}_{nn} (\mathbf{D}_{np} F_s) + \\
& + (\mathbf{D}_{np} F_\tau)^T \widetilde{\mathbf{C}}_{nn} F_s \mathbf{D}_{nx} + (\mathbf{D}_p F_\tau)^T \widetilde{\mathbf{C}}_{pp} (\mathbf{D}_p F_s) + (\mathbf{D}_p F_\tau)^T \widetilde{\mathbf{C}}_{pn} (\mathbf{D}_{np} F_s) + \\
& + (\mathbf{D}_p F_\tau)^T \widetilde{\mathbf{C}}_{pn} F_s \mathbf{D}_{nx} - \mathbf{D}_{nx}^T \widetilde{\mathbf{C}}_{np} F_\tau (\mathbf{D}_p F_s) - \mathbf{D}_{nx}^T \widetilde{\mathbf{C}}_{nn} F_\tau (\mathbf{D}_{np} F_s) - \\
& - \mathbf{D}_{nx}^T \widetilde{\mathbf{C}}_{nn} F_\tau F_s \mathbf{D}_{nx} \Big] d\Omega \, \mathbf{u}_s \, dx - \int_l \delta \mathbf{u}_\tau^T \int_\Omega \Big[(\mathbf{D}_{np} F_\tau)^T \left(\widetilde{\lambda}_n \Theta_\Omega \mathbf{I} \right) + \\
& + (\mathbf{D}_p F_\tau)^T \left(\widetilde{\lambda}_p \Theta_\Omega \mathbf{I} \right) - \mathbf{D}_{nx}^T F_\tau \left(\widetilde{\lambda}_n \Theta_\Omega \mathbf{I} \right) \Big] d\Omega \, \Theta_n \, dx \\
& + \delta \mathbf{u}_\tau^T \int_\Omega F_\tau \left[\widetilde{\mathbf{C}}_{np} (\mathbf{D}_p F_s) + \widetilde{\mathbf{C}}_{nn} (\mathbf{D}_{np} F_s) + \widetilde{\mathbf{C}}_{nn} F_s \mathbf{D}_{nx} \right] d\Omega \, \mathbf{u}_s \Bigg|_{x=0}^{x=l} - \\
& - \delta \mathbf{u}_\tau^T \int_\Omega F_\tau \left(\widetilde{\lambda}_n \Theta_\Omega \mathbf{I} \right) d\Omega \, \Theta_n \Bigg|_{x=0}^{x=l}
\end{aligned} \tag{18}$$

In a compact vectorial form:

$$\begin{aligned}
\delta L_i = & \int_l \delta \mathbf{u}_\tau^T \, \overline{\mathbf{K}}_{uu}^{\tau s} \, \mathbf{u}_s \, dx - \int_l \delta \mathbf{u}_\tau^T \, \overline{\mathbf{K}}_{u\theta}^{\tau} \, \Theta_n \, dx + \\
& + \left[\delta \mathbf{u}_\tau^T \, \overline{\mathbf{\Pi}}_{uu}^{\tau s} \, \mathbf{u}_s \right]_{x=0}^{x=l} - \left[\delta \mathbf{u}_\tau^T \, \overline{\mathbf{\Pi}}_{u\theta}^{\tau} \, \Theta_n \right]_{x=0}^{x=l}
\end{aligned} \tag{19}$$

The components of the differential linear stiffness matrix $\overline{\mathbf{K}}_{uu}^{\tau s}$ are:

$$
\begin{aligned}
\overline{K}_{uu_{xx}}^{\tau s} &= J_{\tau,ys,y}^{66} + J_{\tau,zs,z}^{55} - J_{\tau s}^{11}\frac{\partial^2}{\partial x^2} \quad \overline{K}_{uu_{xy}}^{\tau s} = \left(J_{\tau,ys}^{66} - J_{\tau s,y}^{12}\right)\frac{\partial}{\partial x} \\
\overline{K}_{uu_{yy}}^{\tau s} &= J_{\tau,ys,y}^{22} + J_{\tau,zs,z}^{44} - J_{\tau s}^{66}\frac{\partial^2}{\partial x^2} \quad \overline{K}_{uu_{yx}}^{\tau s} = \left(J_{\tau,ys}^{12} - J_{\tau s,y}^{66}\right)\frac{\partial}{\partial x} \\
\overline{K}_{uu_{zz}}^{\tau s} &= J_{\tau,ys,y}^{44} + J_{\tau,zs,z}^{33} - J_{\tau s}^{55}\frac{\partial^2}{\partial x^2} \quad \overline{K}_{uu_{zx}}^{\tau s} = \left(J_{\tau,zs}^{13} - J_{\tau s,z}^{55}\right)\frac{\partial}{\partial x} \\
\overline{K}_{uu_{xz}}^{\tau s} &= \left(J_{\tau,zs}^{55} - J_{\tau s,z}^{13}\right)\frac{\partial}{\partial x} \\
\overline{K}_{uu_{yz}}^{\tau s} &= J_{\tau,ys,z}^{23} + J_{\tau,zs,y}^{44} \\
\overline{K}_{uu_{zy}}^{\tau s} &= J_{\tau,zs,y}^{23} + J_{\tau,ys,z}^{44}
\end{aligned}
\tag{20}
$$

The generic term $J_{\tau_{(,\phi)}s_{(,\xi)}}^{gh}$ is a cross-section moment:

$$
J_{\tau_{(,\phi)}s_{(,\xi)}}^{gh} = \int_{\Omega} \widetilde{C}_{gh} F_{\tau_{(,\phi)}} F_{s_{(,\xi)}} \, d\Omega \tag{21}
$$

and it is obtained via Gauss' integration.
The components of the differential linear stiffness vector $\overline{\mathbf{K}}_{u\theta}^{\tau}$ are:

$$
\begin{aligned}
\overline{K}_{u\theta_{xx}}^{\tau} &= J_{\tau,y}^{6} + J_{\tau,z}^{5} - J_{\tau}^{1}\frac{\partial}{\partial x} \\
\overline{K}_{u\theta_{yy}}^{\tau} &= J_{\tau,z}^{4} + J_{\tau,y}^{2} - J_{\tau}^{6}\frac{\partial}{\partial x} \\
\overline{K}_{u\theta_{zz}}^{\tau} &= J_{\tau,z}^{3} + J_{\tau,y}^{4} - J_{\tau}^{5}\frac{\partial}{\partial x}
\end{aligned}
\tag{22}
$$

The generic term $J_{\tau_{(,\phi)}}^{g}$ is:

$$
J_{\tau_{(,\phi)}}^{g} = \int_{\Omega} F_{\tau_{(,\phi)}} \, \widetilde{\lambda}_{g} \, \Theta_{\Omega} \, d\Omega \tag{23}
$$

As far as the boundary conditions are concerned, the components of $\overline{\mathbf{\Pi}}_{uu}^{\tau s}$ are:

$$
\begin{aligned}
\overline{\Pi}_{uu_{xx}}^{\tau s} &= J_{\tau s}^{11}\frac{\partial}{\partial x} \quad \overline{\Pi}_{uu_{xy}}^{\tau s} = J_{\tau s,y}^{12} \quad \overline{\Pi}_{uu_{xz}}^{\tau s} = J_{\tau s,z}^{13} \\
\overline{\Pi}_{uu_{yy}}^{\tau s} &= J_{\tau s}^{66}\frac{\partial}{\partial x} \quad \overline{\Pi}_{uu_{yx}}^{\tau s} = J_{\tau s,y}^{66} \quad \overline{\Pi}_{uu_{yz}}^{\tau s} = 0 \\
\overline{\Pi}_{uu_{zz}}^{\tau s} &= J_{\tau s}^{55}\frac{\partial}{\partial x} \quad \overline{\Pi}_{uu_{zx}}^{\tau s} = J_{\tau s,z}^{55} \quad \overline{\Pi}_{uu_{zy}}^{\tau s} = 0
\end{aligned}
\tag{24}
$$

The components of $\overline{\mathbf{\Pi}}_{u\theta}^{\tau}$ are:

$$
\begin{aligned}
\overline{\Pi}_{u\theta_{xx}}^{\tau} &= J_{\tau}^{1} \\
\overline{\Pi}_{u\theta_{yy}}^{\tau} &= J_{\tau}^{6} \\
\overline{\Pi}_{u\theta_{zz}}^{\tau} &= J_{\tau}^{5}
\end{aligned}
\tag{25}
$$

4.2 Governing equations' fundamental nuclei

The fundamental nucleo of the governing equations in a compact vectorial form is:

$$\delta \mathbf{u}_\tau^T : \ \overline{\mathbf{K}}_{uu}^{\tau s} \, \mathbf{u}_s \ - \ \overline{\mathbf{K}}_{u\theta}^{\tau} \, \Theta_{\mathbf{n}} \ = 0 \tag{26}$$

The thermal load can be moved to the right terms:

$$\delta \mathbf{u}_\tau^T : \ \overline{\mathbf{K}}_{uu}^{\tau s} \, \mathbf{u}_s \ = \ \overline{\mathbf{K}}_{u\theta}^{\tau} \, \Theta_{\mathbf{n}} \tag{27}$$

In explicit form:

$$\begin{aligned}
&\delta u_{x\tau} : \\
&-J_{\tau s}^{11} u_{xs,xx} + \left(J_{\tau,zs,z}^{55} + J_{\tau,ys,y}^{66} \right) u_{xs} + \left(J_{\tau,ys}^{66} - J_{\tau s,y}^{12} \right) u_{ys,x} + \\
&+ \left(J_{\tau,zs}^{55} - J_{\tau s,z}^{13} \right) u_{zs,x} = J_{\tau,y}^{6} \Theta_n + J_{\tau,z}^{5} \Theta_n - J_{\tau}^{1} \Theta_{n,x} \\
&\\
&\delta u_{y\tau} : \\
&\left(J_{\tau,ys}^{12} - J_{\tau s,y}^{66} \right) u_{xs,x} - J_{\tau s}^{66} u_{ys,xx} + \left(J_{\tau,ys,y}^{22} + J_{\tau,zs,z}^{44} \right) u_{ys} + \\
&+ \left(J_{\tau,ys,z}^{23} + J_{\tau,zs,y}^{44} \right) u_{zs} = J_{\tau,z}^{4} \Theta_n + J_{\tau,y}^{2} \Theta_n - J_{\tau}^{6} \Theta_{n,x} \\
&\\
&\delta u_{z\tau} : \\
&\left(J_{\tau,zs}^{13} - J_{\tau s,z}^{55} \right) u_{xs,x} + \left(J_{\tau,zs,y}^{23} + J_{\tau,ys,z}^{44} \right) u_{ys} - J_{\tau s}^{55} u_{zs,xx} + \\
&+ \left(J_{\tau,zs,z}^{33} + J_{\tau,ys,y}^{44} \right) u_{zs} = J_{\tau,z}^{3} \Theta_n + J_{\tau,y}^{4} \Theta_n - J_{\tau}^{5} \Theta_{n,x}
\end{aligned} \tag{28}$$

The boundary conditions are:

$$\begin{aligned}
&\delta u_{x\tau} \left(J_{\tau s}^{11} u_{xs,x} + J_{\tau s,y}^{12} u_{ys} + J_{\tau s,z}^{13} u_{zs} - J_{\tau}^{1} \Theta_n \right) \Big|_{x=0}^{x=l} = 0 \\
&\delta u_{y\tau} \left(J_{\tau s,y}^{66} u_{xs} + J_{\tau s}^{66} u_{ys,x} - J_{\tau}^{6} \Theta_n \right) \Big|_{x=0}^{x=l} = 0 \\
&\delta u_{z\tau} \left(J_{\tau s,z}^{55} u_{xs} + J_{\tau s}^{55} u_{zs,x} - J_{\tau}^{5} \Theta_n \right) \Big|_{x=0}^{x=l} = 0
\end{aligned} \tag{29}$$

For a fixed approximation order, the nuclei have to be expanded versus the indexes τ and s in order to obtain the governing equations and the boundary conditions of the desired model.

5 Solution of Fourier's heat conduction equation

If the considered beam is subjected to a sinusoidal thermal load at the top surface ($z = +b/2$) and at the bottom surface ($z = -b/2$), the thermal boundary conditions are:

$$\begin{aligned}
&T = 0 \quad \texttt{at}\ x = 0,\, l \\
&T = T_b \sin\left(\frac{m\pi x}{l} \right) \quad \texttt{at}\ z = -b/2 \ \texttt{with}\ \texttt{b:bottom} \\
&T = T_t \sin\left(\frac{m\pi x}{l} \right) \quad \texttt{at}\ z = +b/2 \ \texttt{with}\ \texttt{t:top}
\end{aligned} \tag{30}$$

where m is the half-wave number along the axis direction x. l is the lenght of the beam and a is the side dimension of the cross-scetion. T_b and T_t are the amplitudes of the temperature at the bottom and top, respectively. We do not consider variation of the temperature respect to the y direction.
In the case of multi-layered structures, continuity conditions for the temperature T and the heat flux q_z hold in the $z-$direction at each $k-$th layer interface:

$$T_t^k = T_b^{k+1} \;\; q_{zt}^k = q_{zb}^{k+1} \;\; \texttt{for}\; k = 1, \ldots, N_l - 1 \tag{31}$$

where N_l is the number of layers of the beam. The relationship between the heat flux and the temperature is:

$$q_z^k = K_3^k \frac{\partial T^k}{\partial z} \tag{32}$$

In general for the $k-$th homogeneous orthotropic layer, the differential Fourier equation of heat conduction is:

$$K_1^k \frac{\partial^2 T}{\partial x^2} + K_3^k \frac{\partial^2 T}{\partial z^2} = 0 \tag{33}$$

considering $T = T(x, z)$. K_1^k and K_3^k are the thermal conductivities along the x and z beam directions. For each layer, both governing equations and boundary conditions are satisfied assuming the following temperature field:

$$T(x, z) = \Theta_\Omega(z) \sin\left(\frac{m\pi x}{l}\right) \tag{34}$$

with $\Theta_\Omega(z) = T_0 \exp\left(s^k z\right)$.
T_0 is a constant and s^k a parameter. Substituting Equation (34) in Equation(33) and solving for s^k, we obtain:

$$s_{1,2}^k = \pm\sqrt{\frac{K_1^k}{K_3^k}} \cdot \frac{m\pi}{l} \tag{35}$$

when the material is isotropic the thermal conductivities can be simplified and $s_{1,2} = \pm\frac{m\pi}{l}$. $\Theta_\Omega(z)$ becomes:

$$\begin{aligned} &\Theta_\Omega(z) = T_{01}^k \exp\left(s_1^k z\right) + T_{02}^k \exp\left(-s_1^k z\right) \\ &\texttt{or} \quad \Theta_\Omega(z) = C_1^k \cosh\left(s_1^k z\right) + C_2^k \sinh\left(s_1^k z\right) \end{aligned} \tag{36}$$

The solution ca be written as:

$$T(x, z) = \left[C_1^k \cosh\left(s_1^k z\right) + C_2^k \sinh\left(s_1^k z\right)\right] \sin\left(\frac{m\pi x}{l}\right) \tag{37}$$

where the unknown coefficients C_1^k and C_2^k are constant for each layer k. If N_l is the number of layer, we have $2N_l$ unknowns and we need $2N_l$ eqautions to determine

them. The temperature at the top and bottom surfaces is known and therefore we have the following two conditions:

$$\begin{aligned} T_b &= C_1^1 \cosh\left(s_1^1 z_b\right) + C_2^1 \sinh\left(s_1^1 z_b\right) \\ T_t &= C_1^{N_l} \cosh\left(s_1^{N_l} z_t\right) + C_2^{N_l} \sinh\left(s_1^{N_l} z_t\right) \end{aligned} \tag{38}$$

Others $N_l - 1$ equations can be obtained from the continuity of temperature at each interface, whereas $N_l - 1$ equations result from the continuity of the heat flux through the interfaces, as writeen in Equation (31). We can write:

$$\begin{aligned} &C_1^k \cosh\left(s_1^k z_t^k\right) + C_2^k \sinh\left(s_1^k z_t^k\right) - C_1^{k+1} \cosh\left(s_1^{k+1} z_b^{k+1}\right) + C_2^{k+l} \sinh\left(s_1^{k+l} z_b^{k+1}\right) = 0 \\ &K_3^k C_1^k s_1^k \sinh\left(s_1^k z_t^k\right) + K_3^k C_2^k s_1^k \cosh\left(s_1^k z_t^k\right) - K_3^{k+1} C_1^{k+1} s_1^{k+1} \sinh\left(s_1^{k+1} z_b^{k+1}\right) + \\ &-K_3^{k+1} C_2^{k+1} s_1^{k+1} \sinh\left(s_1^{k+l} z_b^{k+1}\right) = 0 \end{aligned} \tag{39}$$

In Equation (39), z_t^k and z_b^{k+1} represent the top of the $k-$th layer and the bottom of the $(k+1)-$th layer, respectively. Solving the system given by Equations (38) and (39) we obtain the N_l coeficients C_1^k and C_2^k. Therefore we can compute the temperature at different values of z and x coordinates.

6 Closed form analytical solution

Once the temperature on the beam is computed, the differential equations are solved via a Navier-type solution. Simply supported beams are, therefore, investigated. The following harmonic displacement field is adopted:

$$\begin{aligned} u_x &= F_\tau U_{x\tau} \cos(\alpha x) \\ u_y &= F_\tau U_{y\tau} \sin(\alpha x) \\ u_z &= F_\tau U_{z\tau} \sin(\alpha x) \\ \Theta &= \Theta_\Omega \sin(\alpha x) \end{aligned} \tag{40}$$

where α is:

$$\alpha = \frac{m\pi}{l} \tag{41}$$

$m \in \mathbf{N}^+$ represents the half-wave number along the beam axis. $\{U_{i\tau} : i = x, y, z\}$ are the maximal amplitudes of the displacement components. Upon substitution of

Equations (40) into Equations (28), the fundamental algebraic nucleo is obtained:

$$
\begin{aligned}
&\delta U_{x\tau}: \\
&\left(\alpha^2 J^{11}_{\tau s} + J^{55}_{\tau,zs,z} + J^{66}_{\tau,ys,y}\right) U_{xs} + \alpha\left(J^{66}_{\tau,ys} - J^{12}_{\tau s,y}\right) U_{ys} + \\
&+\alpha\left(J^{55}_{\tau,zs} - J^{13}_{\tau s,z}\right) U_{zs} = J^{6}_{\tau,y} + J^{5}_{\tau,z} - \alpha J^{1}_{\tau} \\
&\delta U_{y\tau}: \\
&\alpha\left(J^{66}_{\tau s,y} - J^{12}_{\tau,ys}\right) U_{xs} + \left(\alpha^2 J^{66}_{\tau s} + J^{22}_{\tau,ys,y} + J^{44}_{\tau,zs,z}\right) U_{ys} + \\
&+\left(J^{23}_{\tau,ys,z} + J^{44}_{\tau,zs,y}\right) U_{zs} = J^{4}_{\tau,z} + J^{2}_{\tau,y} - \alpha J^{6}_{\tau} \\
&\delta U_{z\tau}: \\
&\alpha\left(J^{55}_{\tau s,z} - J^{13}_{\tau,zs}\right) U_{xs} + \left(J^{23}_{\tau,zs,y} + J^{44}_{\tau,ys,z}\right) U_{ys} + \\
&+\left(\alpha^2 J^{55}_{\tau s} + J^{33}_{\tau,zs,z} + J^{44}_{\tau,ys,y}\right) U_{zs} = J^{3}_{\tau,z} + J^{4}_{\tau,y} - \alpha J^{5}_{\tau}
\end{aligned}
\tag{42}
$$

7 Numerical results and discussion

7.1 Isotropic material

Isotropic beams made of an alluminium alloy are first considered. The mechanical properties are: $E = 72$ GPa, $\nu = 0.3$, $K = 121$ W/m°C, $\widetilde{\alpha} = 23 \cdot 10^{-6}$ °C^{-1}. Square cross-sections are considered. The sides of the cross-section are $a = b = 0.1$ m. The length-to-side ratio l/b is equal to 100, ten and five. Slender and deep beams are, therefore, investigated. The half-wave number m in Equation (41) is assumed equal to one. The thermal boundary conditions are: $T_b = 25°C$ and $T_t = 500°C$. Displacements and stresses are evaluated in the following points:

$$
\begin{aligned}
&u_x \texttt{ at } (l, -a/2, b/2) \quad u_y \texttt{ at } (l/2, 0, b/2) \quad u_z \texttt{ at } (l/2, a/2, b/2) \\
&\sigma_{xx} \texttt{ at } (l/2, 0, a/2) \quad \sigma_{xz} \texttt{ at } (0, -a/2, 0) \quad \sigma_{zz} \texttt{ at } (l/2, -a/2, 0)
\end{aligned}
\tag{43}
$$

Results are reported in Tables 1- 5 and in Figures 2- 6.

	u_z	$u_x \times -10^2$	$u_y \times 10^4$
FEM 3D^a	1.1074	3.6608	5.7491
FEM 3D^b	1.1074	3.6608	5.7480
$N \geq 6$	1.1074	3.6608	5.7499
$N = 3 - 5$	1.1074	3.6608	5.7498
$N = 2$	1.1074	3.6607	5.7496
TB	2.4480	8.0953	–
EB	2.4480	8.0951	–

a: mesh 50x20x20
b: mesh 50x10x10

Table 1: Displacements ([m]), isotropic beam, $l/b = 100$

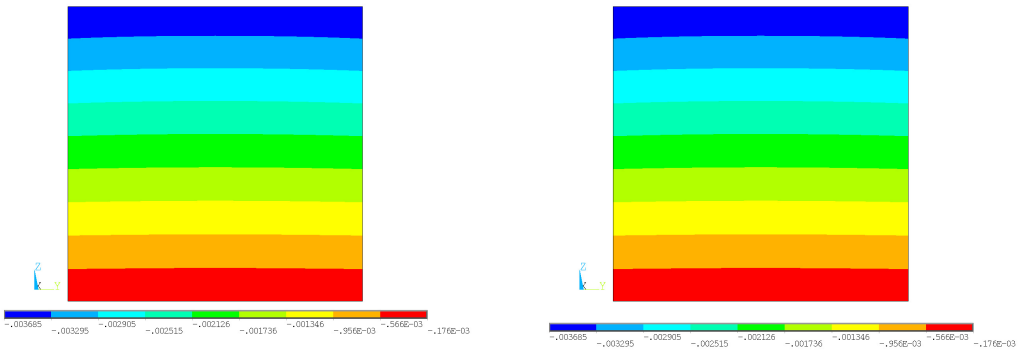

(a) (b)

Figure 2: Axial displacement u_x ([m]), isotropic beam, $l/b = 10$ via (a) FEM 3-D solution and (b) $N = 8$ model

As far as validation is concerned, results are compared with three-dimensional FEM solutions obtained via the commercial code ANSYS®. The accuracy of the three-dimensional FEM solution depends upon the FEM numerical approximation. In order to present the convergence of the three-dimensional reference solution, for each case two different meshes are considered. Acronym FEM 3D^a stand for a three-dimensional FEM model with 50 elements along the axial direction and 20 elements along y and z directions. A coarser solution FEM 3D^b ($50 \times 10 \times 10$ elements) is also considered. Although the three-dimensional FEM solution and the analytical one are different in nature, some considerations about computational time and effort can be addressed. For the reference FEM simulations, the computational time is as high as about 20 minutes (refined mesh) and as low as 5 minutes (coarsest mesh). In the case of the proposed analytical solutions, the computational time is few second regardless the considered approximation order. For slender beams, low expansion orders results match already the FEM solutions for displeacements, whereas for stresses, higher ex-

	$u_z \times 10^2$	$u_x \times -10^3$	$u_y \times 10^4$
FEM 3D^a	1.1511	3.6847	5.7362
FEM 3D^b	1.1511	3.6847	5.7362
$N \geq 9$	1.1511	3.6847	5.7362
$N = 8$	1.1511	3.6848	5.7362
$N = 7$	1.1511	3.6848	5.7361
$N = 6$	1.1511	3.6845	5.7356
$N = 5$	1.1511	3.6845	5.7349
$N = 4$	1.1513	3.6868	5.7337
$N = 3$	1.1513	3.6868	5.7330
$N = 2$	1.1501	3.6757	5.7111
TB	2.4440	8.0546	–
EB	2.4440	8.0546	–

a: mesh 50x20x20
b: mesh 50x10x10

Table 2: Displacements ([m]), isotropic beam, $l/b = 10$

pansion orders are required. This behavior becomes more evident for deep beams. $N = 9$ or 11 is necessary to obtain good results for displacements when l/b is 10 and 5. For stresses, the higher expansion orders are necessary even for deep beams. Classical theories provide very poor results if compared with those obteined via higher-order models.

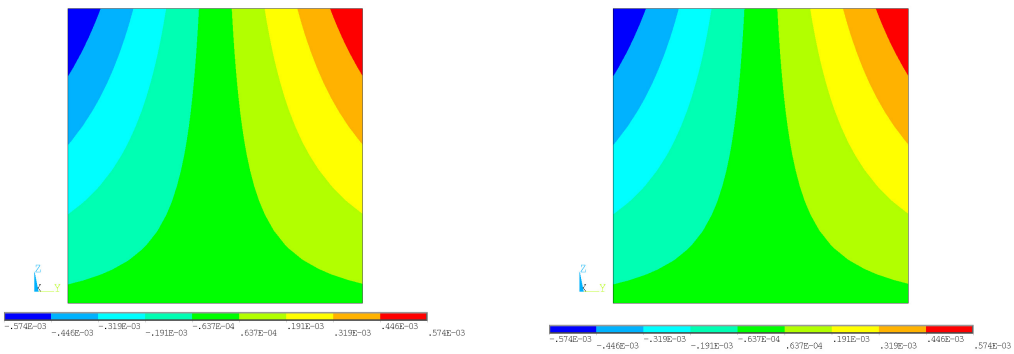

(a) (b)

Figure 3: Transverse displacement u_y ([m]), isotropic beam, $l/b = 10$ via (a) FEM 3-D solution and (b) $N = 8$ model

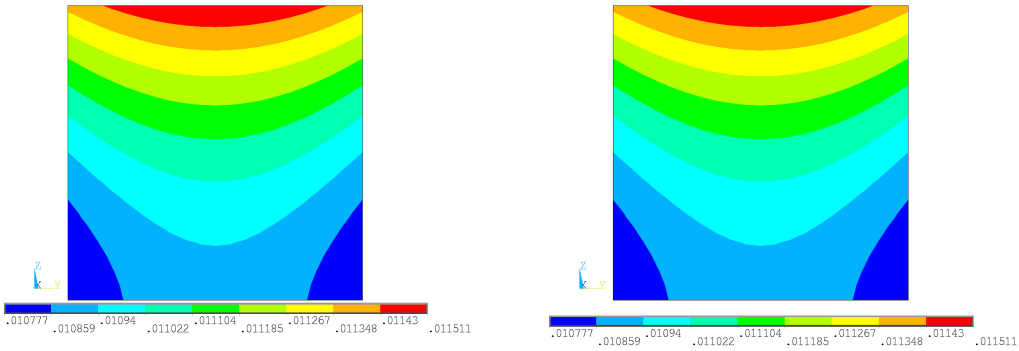

(a) (b)

Figure 4: Transverse displacement u_z ([m]), isotropic beam, $l/b = 10$ via (a) FEM 3-D solution and (b) $N = 8$ model

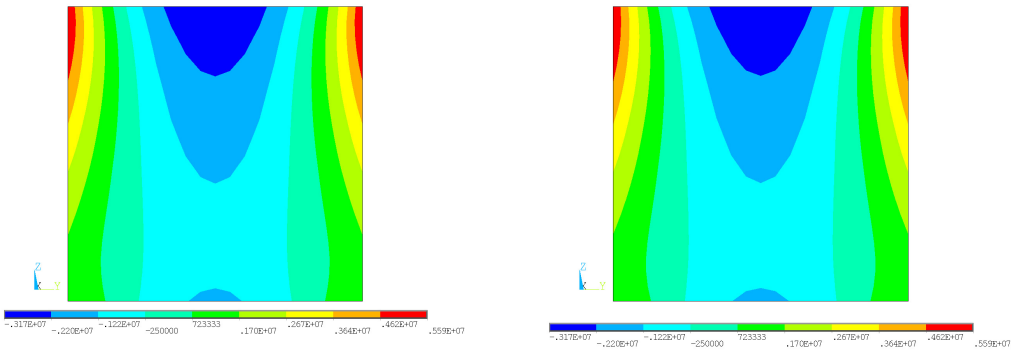

(a) (b)

Figure 5: Axial stress σ_{xx} ([GPa]), isotropic beam, $l/b = 10$ via (a) FEM 3-D solution and (b) $N = 8$ model

	$\sigma_{xx} \times -10^{-6}$	$\sigma_{xz} \times -10^{-7}$	$\sigma_{zz} \times -10^{-6}$
FEM 3D^a	3.1717	1.4860	1.6574
FEM 3D^b	3.2093	1.4745	1.6333
$N = 13$	3.1560	1.4898	1.6657
$N = 12$	3.1620	1.4920	1.6690
$N = 11$	3.1664	1.4920	1.6690
$N = 10$	3.1627	1.4812	1.6753
$N = 9$	3.1642	1.4813	1.6755
$N = 8$	3.1342	1.4859	1.6844
$N = 7$	3.1106	1.4860	1.6841
$N = 6$	3.2221	1.5843	1.5441
$N = 5$	2.9749	1.5841	1.5398
$N = 4$	3.3527	1.3100	1.0496
$N = 3$	4.1150	1.3100	1.0518
$N = 2$	8.0406	1.1822	-5.4328
TB	-993.90	$-$	$-$
EB	-993.90	$-$	$-$

a: mesh 50x20x20
b: mesh 50x10x10

Table 3: Stresses ([Gpa]), isotropic beam, $l/b = 10$

	$u_z \times 10^3$	$u_x \times -10^3$	$u_y \times 10^4$
FEM 3D^a	3.2029	1.8774	5.6949
FEM 3D^b	3.2029	1.8774	5.6949
$N \geq 11$	3.2029	1.8774	5.6949
$N = 10$	3.2029	1.8774	5.6948
$N = 9$	3.2029	1.8774	5.6948
$N = 8$	3.2029	1.8775	5.6946
$N = 7$	3.2029	1.8775	5.6942
$N = 6$	3.2029	1.8770	5.6922
$N = 5$	3.2030	1.8770	5.6894
$N = 4$	3.2044	1.8813	5.6846
$N = 3$	3.2046	1.8813	5.6818
$N = 2$	3.1910	1.8599	5.5971
TB	6.0802	3.9679	$-$
EB	6.0802	3.9679	$-$

a: mesh 50x20x20
b: mesh 50x10x10

Table 4: Displacements ([m]), isotropic beam, $l/b = 5$

	$\sigma_{xx} \times 10^{-7}$	$\sigma_{xz} \times 10^{-7}$	$\sigma_{zz} \times 10^{-6}$
FEM 3D^a	1.2257	2.9092	6.3141
FEM 3D^b	1.2401	2.8857	6.2204
$N = 13$	1.2197	2.9168	6.3462
$N = 12$	1.2221	2.9214	6.3588
$N = 11$	1.2239	2.9214	6.3587
$N = 10$	1.2225	2.8999	6.3826
$N = 9$	1.2228	2.9000	6.3859
$N = 8$	1.2111	2.9096	6.4232
$N = 7$	1.2012	2.9102	6.4186
$N = 6$	1.2425	3.1042	5.9066
$N = 5$	1.1526	3.1025	5.8409
$N = 4$	1.3072	2.5603	3.9693
$N = 3$	1.6096	2.5605	4.0041
$N = 2$	3.0914	2.3297	-20.949
TB	96.706	–	–
EB	96.706	–	–

a: mesh 50x20x20
b: mesh 50x10x10

Table 5: Stresses ([Gpa]), isotropic beam, $l/b = 5$

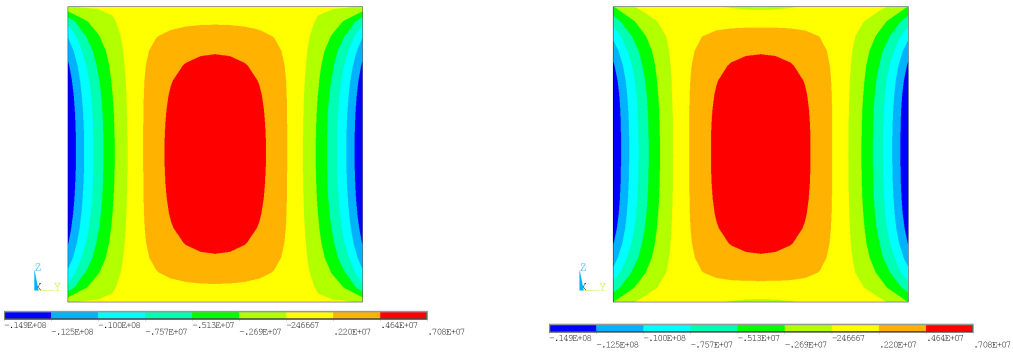

(a) (b)

Figure 6: Shear stress σ_{xz} ([GPa]), isotropic beam, $l/b = 10$ via (a) FEM 3-D solution and (b) $N = 8$ model

Figures 2- 6 show the displacements and stresses fields at the beam cross-section in $x = 0$ or $x = l/2$. The considered expansion order is $N = 8$ and the slenderness ratio is $l/b = 10$. In general, $N = 8$ is sufficient to achieve a good overall solution along the cross-section of the beam, while in tables there is a set set of punctul values, and then higher orders of expansion are necessary to reduce the error.

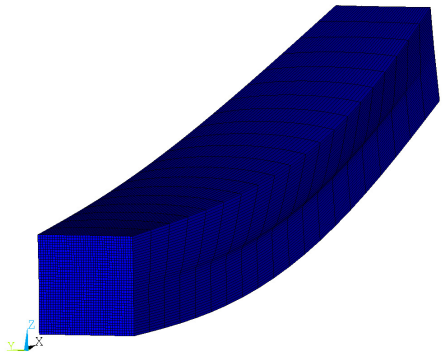

Figure 7: Deformation of the beam, $l/b = 10$

7.2 Orthotropic material

Composite beams are considered in this section. The mechanical properties are: $E_L = 172.72 \times 10^9$ Pa, $E_T = 6.91 \times 10^9$ Pa, $G_{LT} = 3.45 \times 10^9$ Pa, $G_{TT} = 1.38 \times 10^9$ Pa, $\nu_{LT} = \nu_{TT} = 0.25$, $K_L = 36.42$ W/mK, $K_T = 0.96$ W/mK, $\widetilde{\alpha}_L = 0.57 \cdot 10^{-6}\text{K}^{-1}$, $\widetilde{\alpha}_T = 35.60 \cdot 10^{-6}\text{K}^{-1}$. A two layers [0/90] lamination, starting from the bottom, is considered. Square cross-sections are considered. The sides of the cross-section are $a = b = 1$ m. The length-to-side ratio l/b is equal to ten. The thermal boundary conditions are: $T_b = 0$ K and $T_t = 1$ K. In Figure 7 is reported the deformed shape of the beam. The behavior after deformation is due to the 90 $^\circ$ layer that is on the top of the beam and has a small value of $\widetilde{\alpha}_L$. Results for displacements and stresses are presented in Figure 8. Higher-order models result necessary when we consider composite beams. From the pictures we notice that at the interface of the two layers we have the higher errors, compared to the FEM3D solution. A layer-wise approach could better identify the behavior of the beam.

8 Conclusions

A unified formulation of one-dimensional beam models has been proposed for the thermal analysis of isotropic and composite beams. Results have been validated through comparison with three-dimensional FEM solutions obtained via the commercial code ANSYS. On the basis of the presented results, it can be concluded that the proposed formulation allows obtaining results as accurate as desired through an appropriate choice of the approximation order. The efficiency of the proposed models is very high since the computational time is few second for the highest considered approximation order, whereas the three-dimensional FEM solution can require 20 minutes.

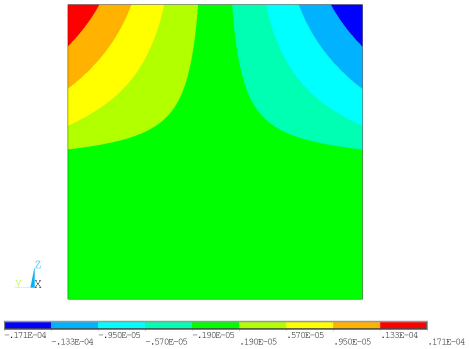

(a) u_y (m), FEM3D solution

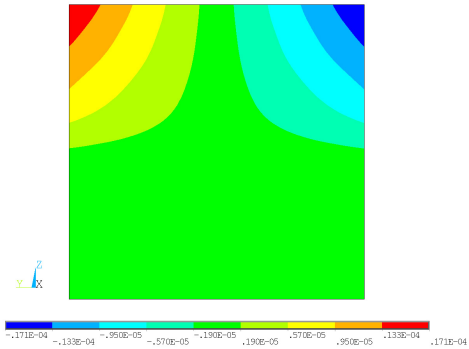

(b) u_y (m), N=15

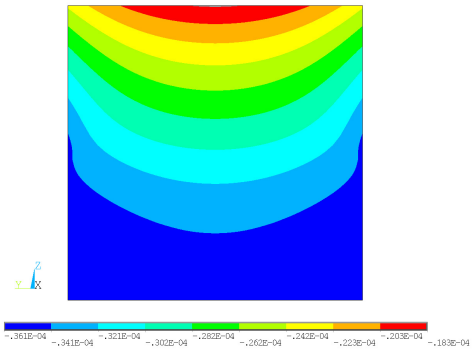

(c) u_z (m), FEM3D solution

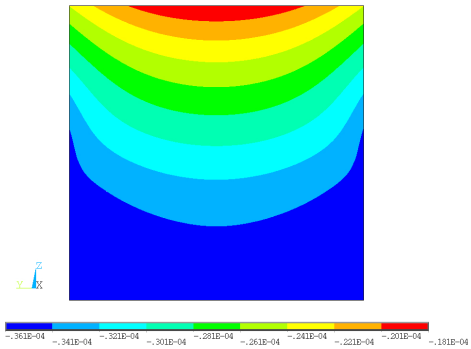

(d) u_z (m), N=15

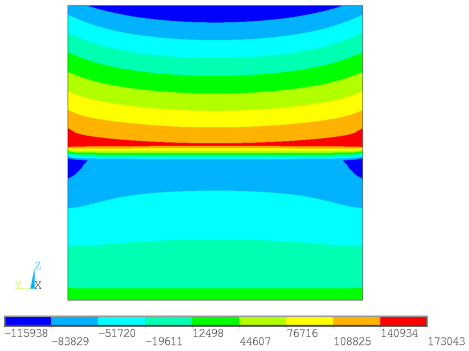

(e) σ_{xx} (Pa), FEM3D solution

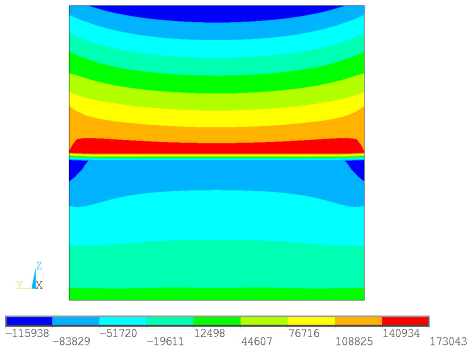

(f) σ_{xx} (Pa), N=20

Figure 8: Composite beam, $l/b = 10$

Acknowledgments

First and second authors are supported by the Fonds National de la Recherche of Luxembourg (FNR) via the AFR grant PHD-MARP-03 and the project CORE C09/MS/05 FUNCTIONALLY, respectively.

References

[1] R.B. Hetnarski, M. R. Eslami, "Thermal stresses - Advanced theory and applications", Springer, 2009.

[2] A.Carpinteri, M.Paggi, "Thermo-elastic mismatch in nonhomogeneous beams", Journal of Engineering Mathematics, 61, 371-384, 2008.

[3] G.L. Ghiringhelli, "On the thermanl problem for composite beams using a finite element semi-discretisation", Composite Part B, 28, 483–495, 1997.

[4] Y.Xu, D.Zhou, "Two-dimensional thermoelastic analysis of beams with variable thickness subjected to thermo-mechanical loads", Applied Mathematical Modelling, doi: 10.1016/j.apm.2012.01.048, 2012.

[5] P.Vidal, O.Polit, "A thermomechanical finite element for the analysis of rectangular laminated beams", Finite Elements in Analysis and Design, 42, 868-883, 2006.

[6] S.Kapuria, P.C.Dumir, A.Ahmed, "An efficient higher order zigzag theory for composite and sandwich beams subjected to thermal loading", International Journal of Solids and Structures, 40, 6613-6631, 2003.

[7] Y.Tanigawa, H.Murakami, Y.Ootao, "Transient thermal stress analysis of a laminated composite beam", Journal of Thermal Stresses, 12(1), 25-39, 1989.

[8] O.Sayman, "An elastic-plastic thermal stress analysis of aluminum metal-matrix composite beams", Composite Structures, 53, 419-425, 2001.

[9] E.Carrera, "An assessment of mixed and classical theories for the thermal analyis of orthotropic multilayered plates", Journal of Thermal Stresses, 23, 797-831, 2000.

[10] E.Carrera, "Tempertaure profile infulence on layered plates response considering clasical and advanced theories", AIAA Journal, 40, 1885-1896, 2002.

[11] E.Carrera, "Theories and finite elements for multilayered plates and shells: a unified compact formulation with numerical assessment and benchmarking", Archives of Computational Methods in Engineering, 10, 215-296, 2003.

[12] E.Carrera, G.Giunta, M.Petrolo, "Beam Structures: Classical and Advanced Theories", John Wiley & Sons, 2011.

[13] A.Catapano, G.Giunta, S.Belouettar, E.Carrera, "Static analysis of laminated beams via a unified formulation", Composite Structures, 94, 75-83, 2011.

[14] G.R.Cowper. "The shear co-efficient in timoshenko beam theory", Journal of Applied Mechanics, 33(10), 335-340, 1966.

[15] A.V.K.Murty, "Analysis of short beams" AIAA Journal, 8(11), 2098-2100, 1970.

[16] E.Carrera, S.Brischetto, “Analysis of thickness locking in classical, refined and mixed multilayered plate theories”, Composite Structures, 82(4), 549-562, 2008.
[17] E.Carrera, S.Brischetto, “Analysis of thickness locking in classical, refined and mixed theories for layered shells”, Composite Structures, 85(1), 83-90, 2008.